Mon. Not. R. Astron. Soc. **000**, 000–000 (0000) Printed 7 June 2012 (MN LaTeX style file v2.2)

# The Dynamical State and Mass-Concentration Relation of Galaxy Clusters

Aaron D. Ludlow[1,⋆], Julio F. Navarro[2], Ming Li[3], Raul E. Angulo[3], Michael Boylan-Kolchin[4], and Philip E. Bett[1],

[1] *Argelander-Institut für Astronomie, Auf dem Hügel 71, D-53121 Bonn, Germany*
[2] *Dept. of Physics and Astronomy, University of Victoria, Victoria, BC, V8P 5C2, Canada*
[3] *Max-Planck-Institut für Astrophysik, Karl-Schwarzschild-Straße 1, 85740 Garching bei München, Germany*
[4] *Center for Galaxy Evolution, 4129 Reines Hall, University of California, Irvine, CA 92697, USA*

arXiv:1206.1049v1 [astro-ph.CO] 5 Jun 2012

7 June 2012

**ABSTRACT**

We use the Millennium Simulation series to study how the dynamical state of dark matter halos affects the relation between mass and concentration. We find that a large fraction of massive systems are identified when they are substantially out of equilibrium and in a particular phase of their dynamical evolution: the more massive the halo, the more likely it is found at a transient stage of high concentration. This state reflects the recent assembly of massive halos and corresponds to the first pericentric passage of recently-accreted material when, before virialization, the kinetic and potential energies reach maximum and minimum values, respectively. This result explains the puzzling upturn in the mass-concentration relation reported in recent work for massive halos; indeed, the upturn disappears when only dynamically-relaxed systems are considered in the analysis. Our results warn against applying simple equilibrium models to describe the structure of rare, massive galaxy clusters and urges caution when extrapolating scaling laws calibrated on lower-mass systems, where such deviations from equilibrium are less common. The evolving dynamical state of galaxy clusters ought to be carefully taken into account if cluster studies are to provide precise cosmological constraints.

**Key words:**

## 1 INTRODUCTION

Galaxy clusters are powerful cosmological probes. Because of their large masses, they can be detected at cosmological distances despite being rare and studied at various wavelengths, from X-rays to optical to millimeter wavelengths. Their rarity is actually a strength when it comes to cosmology; massive clusters trace the tail of high-mass objects able to collapse under their own gravity and therefore their numbers, as a function of mass and redshift, are exponentially sensitive to the normalization of the power spectrum of density fluctuations and to the cosmological parameters that govern the universal expansion history (see, e.g., Allen et al. 2011, for a recent review and a complete list of references).

Cluster counts are thus widely recognized as a premier tool able to provide cosmological constraints complementary to those based on analysis of the cosmic microwave background, supernova luminosity distances, galaxy clustering, and gravitational lensing (see, e.g., Mantz et al. 2008; Cunha et al. 2009; Henry et al. 2009; Rozo et al. 2009; Vikhlinin et al. 2009). Their potential is more directly realized, however, when observables can be turned into effective measures of cluster mass; indeed, the most robust and discriminating theoretical predictions concern the abundance and redshift evolution of clusters of different mass.

Mass, however, is not directly observable, which means in practice that observables such as cluster richness, velocity dispersion, X-ray luminosity/temperature, or Sunyaev-Zel'dovich (SZ) decrement must be related to mass through scaling laws whose shape and scatter need careful calibration. Although virial equilibrium and self-similarity suggest power-law scalings between mass and observational proxies (Kaiser 1986; Navarro et al. 1995), it has long been appreciated that baryon physics breaks self-similarity and imposes scalings with different slopes and redshift dependence (e.g., Kaiser 1991; Evrard & Henry 1991).

⋆ E-mail:aludlow@astro.uni-bonn.de

The complexity of the baryon physics involved precludes robust theoretical predictions and therefore the mass-observable relations are usually parameterized as power laws of adjustable slope, redshift-dependent normalization, and Gaussian scatter that are empirically calibrated using a (usually small) set of well-studied clusters. Besides simplicity, the underlying rationale of this procedure is that, however intricate, the mass-dependence of the physical processes responsible for a given mass-observable relation is monotonic and that deviations of individual clusters from the mean trends are driven by stochastic effects.

The validity of these assumptions, however, is not assured and recent work has highlighted their limitations. One example is the mismatch between the average SZ signal at given optical richness measured by the Planck satellite and expectations based on the X-ray properties of clusters with weak lensing-calibrated masses (Planck Collaboration et al. 2011). This might either indicate a dichotomy in the gas content of clusters of different mass or perhaps arises from the large, correlated scatter between observables suggested by recent simulation work (see, e.g., Angulo et al. 2012).

A second example is provided by recent reports of a non-monotonic relation between the mass and concentration of massive dark matter halos (Klypin et al. 2011; Prada et al. 2011). These authors report an "upturn" in the *median* concentration on mass scales where the rms fluctuations of the linear density field, $\sigma(M,z) \lesssim 1/2$. This corresponds to rare objects with virial masses equivalent to a few times $10^{15}\,M_\odot$ at $z=0$, shifting to lower masses at higher redshift.

The origin of the upturn is unclear. Since halo concentration reflects the mean density of the universe at the time of assembly (Navarro et al. 1996, 1997; Eke et al. 2001; Bullock et al. 2001; Wechsler et al. 2002; Zhao et al. 2003), the mass-concentration relation is expected to be a monotonic one where concentration decreases with increasing halo mass. An upturn in concentration may have non-negligible consequences on cluster studies: concentration is a measure of the characteristic density of a cluster, and it could therefore affect directly mass proxies that are sensitive to density, such as X-ray luminosity. A non-monotonic mass-concentration relation might thus lead to selection biases or "breaks" in the relation between X-ray properties and mass that would be poorly captured by the assumed power-law scalings.

We use here data from the Millennium Simulation series to revisit the mass-concentration relation of rare, massive halos. In particular, we examine the physical origin of the reported "upturn" in concentration and the nature of the scatter about the mean relation. We describe briefly the numerical simulations in Sec. 2, present our results in Sec. 3, and summarize our main conclusions in Sec. 4.

## 2 NUMERICAL SIMULATIONS

### 2.1 The Millennium Simulation series

We use in our analysis halos identified in the three "Millennium Simulations", which we refer to as MS-I, MS-II, and MS-XXL, or collectively as MS. All MS runs adopted the same cosmology (a WMAP-1 normalized flat ΛCDM model) and the same sequence of outputs times in order to facilitate comparisons between the runs. The values of the cosmological parameters are as follows: $\Omega_{\rm m} = 0.25$, $\Omega_\Lambda = 1-\Omega_{\rm m} = 0.75$, $h = 0.73$, $n = 1$ and $\sigma_8 = 0.9$. Here $\Omega_i$ is the present-day contribution of component $i$ to the universal matter energy density in units of the critical density for closure; $\sigma_8$ is the rms mass fluctuation in spheres of $8\,h^{-1}$ Mpc radius linearly extrapolated to $z=0$; $n$ is the spectral index of primordial density fluctuations, and $h$ is the Hubble parameter defined so that $H_0 = H(z=0) = 100\,h$ km/s/Mpc.

The MS-I used $2160^3$ particles of mass $m_p = 8.61\times 10^8\ h^{-1}M_\odot$ to follow the evolution of the dark matter component in a periodic box 500 $h^{-1}$Mpc on a side (Springel et al. 2005). MS-II used the same number of particles, but a box size 5 times smaller, $L_{\rm box} = 100\ h^{-1}$Mpc (Boylan-Kolchin et al. 2009); each MS-I particle is thus 125× heavier than in MS-II. The MS-XXL is substantially larger than MS-I, both in box size ($L_{\rm box} = 3\,h^{-1}$Gpc) and total particle number ($6720^3$), and thus provides the best statistics for the rarest and most massive objects at any redshift (Angulo et al. 2012), albeit with poorer mass resolution. The particle mass in the XXL is $m_p = 6.17\times 10^9\,h^{-1}M_\odot$. The Plummer-equivalent gravitational softening lengths used in these runs are $\epsilon_P = 5\,h^{-1}$kpc (MS-I), $1\,h^{-1}$kpc (MS-II), and $10\,h^{-1}$kpc (MS-XXL).

### 2.2 Analysis

Halos in the MS are identified using a friends-of-friends (FOF) group finder (Davis et al. 1985) with a linking length equal to 20% of the mean interparticle separation. Substructure in each FOF group is identified using SUBFIND (Springel et al. 2001). We consider in our analysis only the main halo of each FOF grouping, and define its virial mass, $M_{200}$, as the mass contained within a sphere centered at the potential minimum that encloses a mean overdensity of 200 times the critical density for closure, $\rho_{\rm crit} = 3H(z)^2/8\pi G$. This implicitly defines the virial radius of a halo, $r_{200}$, and its virial velocity, $V_{200} = \sqrt{GM_{200}/r_{200}}$.

We adopt two different quantities to estimate halo concentrations, $c$. One uses the ratio of the peak circular speed, $V_{\rm max}$, to the virial velocity, $V_{200}$, as in Prada et al. (2011). Concentrations are derived from $V_{\rm max}/V_{200}$ assuming that the mass profile follows the NFW formula (Navarro et al. 1996, 1997). We use *all* particles within $r_{200}$ to estimate $c$; i.e., $V_{\rm max}$ is computed without subtracting substructure. This is important in order to ensure convergence on the overlapping mass scales of different MS runs because substructure, which may affect the estimates, is particularly sensitive to numerical resolution[1].

Some advantages of this estimator include the fact that it is simple to compute, fairly stable numerically ($V_{\rm max}$ is well defined and robustly estimated even at modest numerical resolution), and that it does not rely on profile fitting and residual-minimization techniques. The main disadvantage is that, because it assumes an NFW profile, it is unduly sensitive when $V_{\rm max}$ approaches $V_{200}$: for example, when con-

[1] The slight concentration mismatch betwen MS-I and MS-II halos reported by Prada et al. (2011) is in all likelihood due to this effect (see Fig. 1).

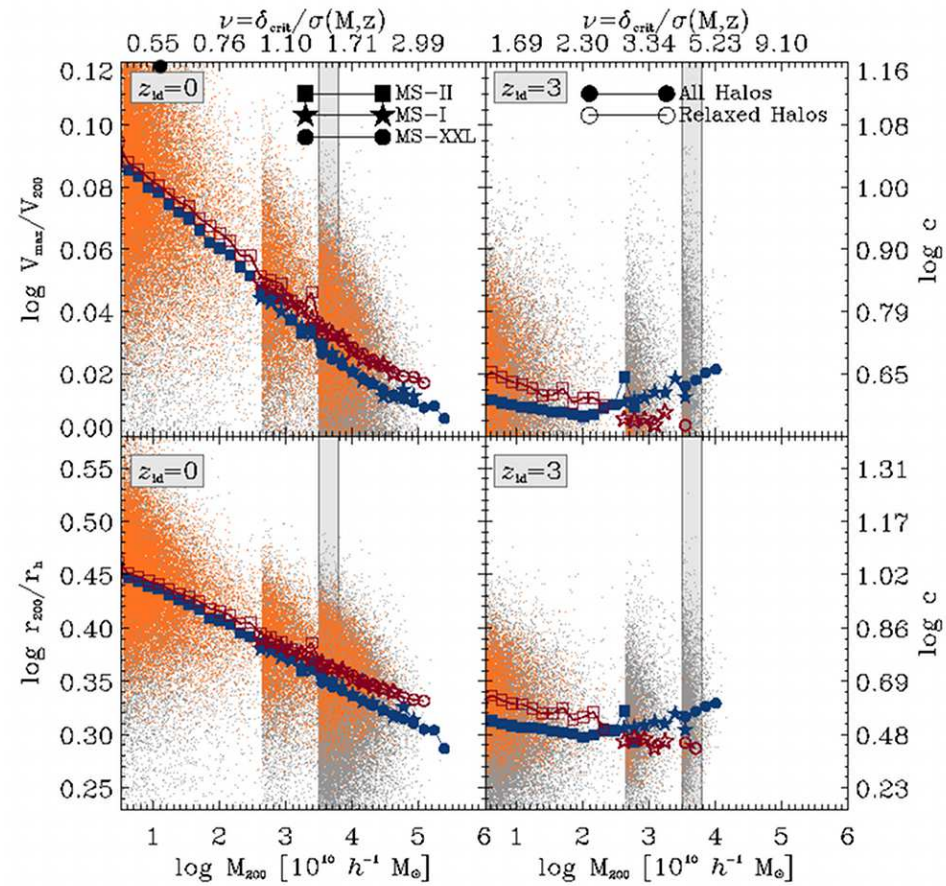


**Figure 1.** Mass-concentration relation for all halos resolved with more than 5000 particles in the Millennium Simulations. The top panels show, as a function of virial mass, concentrations estimated via $V_{\rm max}/V_{200}$, the ratio between the maximum circular velocity and the virial velocity of a halo. Bottom panels show concentrations estimated by the ratio between the half-mass radius and virial radius, $r_{200}/r_{\rm h}$. For each set of panels, the corresponding NFW concentration values are indicated by the right-hand side tickmarks. Panels on the left correspond to halos identified at $z_{\rm id} = 0$, those on the right at $z_{\rm id} = 3$. The three groups of points in each panel correspond, from left to right, to MS-II, MS-I and MS-XXL halos, respectively. All halos are shown in grey, relaxed halos in orange. Connected symbols (see legends) indicate the median concentration computed in bins of virial mass. Open and filled symbols correspond to "relaxed" or all halos, respectively. Note the excellent agreement in the median concentration of halos of similar mass identified in different simulations. The bottom tickmarks indicate halo virial mass; those at the top the dimensionless mass measure, $\nu = \delta_{\rm crit}/\sigma(M, z)$. Note that, because of the fixed comoving box size of each run, halos identified at $z = 3$ sample "rarer" peaks in the mass spectrum (i.e., higher values of $\nu$) than those at $z = 0$.

centrations double from $c = 2.5$ to 5 $V_{\rm max}/V_{200}$ changes only from 1.001 and 1.062, respectively. Even tiny changes in $V_{\rm max}$ may thus lead to large variations in the derived concentration. Further, a large value of $V_{\rm max}/V_{200}$ does not necessarily imply a high central concentration of matter. For example, a massive substructure may elevate $V_{\rm max}$ but, if located at the outskirts of the halo, it might actually *decrease* the average central density of a halo.

Because of this, we adopt an additional concentration estimator: the virial-to-half mass radius ratio, $r_{200}/r_{\rm h}$, provides a more reliable tracer of the concentration of dark matter. As for the velocity ratio, we use *all* particles within $r_{200}$ to compute $r_{\rm h}$ and express the ratio as a concentration, $c$, assuming an NFW profile.

Our analysis considers all halos resolved with at least 5000 particles (i.e., $N_{200} \geqslant 5000$) at three different redshifts, 0, 1, and 3. This corresponds to a minimum mass of $3.44 \times 10^{10}\ h^{-1} M_\odot$ for MS-II, $4.30 \times 10^{12}\ h^{-1} M_\odot$ for MS-I, and $3.09 \times 10^{13} h^{-1} M_\odot$ for MS-XXL. There is a fairly large overlap in the mass scales covered by the different simulations, which allows us to check the sensitivity of our results to numerical resolution.

As discussed by Neto et al. (2007), halo concentrations can be affected by transient departures from equilibrium. We therefore identify a subsample of "relaxed" halos, as those that satisfy the following three criteria: (i) $f_{\rm sub} < 0.1$, (ii) $d_{\rm off} < 0.07$ and (iii) $2T/|U| < 1.3$. Here $f_{\rm sub} = M_{\rm sub}/M_{200}$ is the mass fraction contributed by substructure; $d_{\rm off} = |\mathbf{r}_p - \mathbf{r}_{\rm CM}|/r_{200}$ is the offset between the position of the potential minimum and the halo barycenter, expressed in units

of the virial radius; and $2T/|U|$ is the virial ratio of kinetic to potential energies. We refer the reader to Neto et al. (2007) for further discussion of these criteria. The total number of halos considered in each simulation, as well as the total number of relaxed halos, are listed for each redshift in Table 1.

## 3 RESULTS

### 3.1 Mass-concentration relation

Figure 1 shows, as a function of virial mass, the concentration of halos in our sample, as measured by $V_{\rm max}/V_{200}$ (top panels) or $r_{200}/r_{\rm h}$ (bottom panels). Tickmarks on the right express these quantities in terms of NFW-based concentration values. All individual halos are shown by grey dots; those that pass the three relaxation criteria are shown in orange. Panels on the left show halos identified at $z_{\rm id} = 0$; those on the right correspond to $z_{\rm id} = 3$. Median concentrations for all (blue) and relaxed (red) halos are shown by connected symbols (see legend on figure for identification). The excellent agreement between the different runs on overlapping mass scales indicates that our results are unaffected by numerical resolution effects.

The results for *all* halos shown in Fig. 1 confirm the upturn in the median concentration of massive halos reported by Klypin et al. (2011) and Prada et al. (2011). As discussed by these authors, the upturn affects only rare, extremely massive systems, and is therefore more easily appreciated at earlier times in simulations of fixed comoving box size (i.e., $z_{\rm id} = 3$ in Fig. 1), when massive halos trace rarer peaks of the density fluctuation field. We quantify this using the dimensionless "peak height" mass parameter

$$\nu(M, z) = \delta_{\rm crit}(z)/\sigma(M, z), \quad (1)$$

defined as the ratio between the critical overdensity for collapse at redshift $z$ and the linear rms fluctuation at $z$ within spheres containing mass $M$. The larger the value of $\nu$, the rarer the halo and the more massive it is relative to the characteristic clustering mass ($M_*$) at that epoch, which is usually defined by the condition $\nu(M_*) = 1$. Tickmarks along the top of Fig. 1 list the values of $\nu$ corresponding to the virial masses listed along the bottom axes. At $z = 0$ even the MS-XXL can only probe the regime $\nu < 3$, whereas at $z = 3$ massive halos trace peaks as rare as $\nu \sim 5$. These objects are considerably rarer than those probed by Prada et al. (2011) ($\nu \lesssim 4$), reflecting the extremely large volume of MS-XXL.

Interestingly, the upturn disappears when only "relaxed" halos are considered, a clear indication that out-of-equilibrium effects are responsible. This seems at odds with Prada et al. (2011), who argue that the upturn remains even when unrelaxed halos are excluded; however, they use less restrictive relaxation criteria than the ones we adopt here. In particular, Prada et al use $d_{\rm off} < 0.1$ and $2T/|U| < 1.5$, compared with our adopted values of 0.07 and 1.3, respectively, which are based on the work of Neto et al. (2007). These relatively small differences in the criteria have a large effect on the massive halo sample. For example, at $z = 3$ fewer than $\sim 3\%$ of MS-XXL halos in the sample satisfy our offset and virial ratio criteria; on the other hand, 61% of them pass the less restrictive criteria adopted by Prada et al.

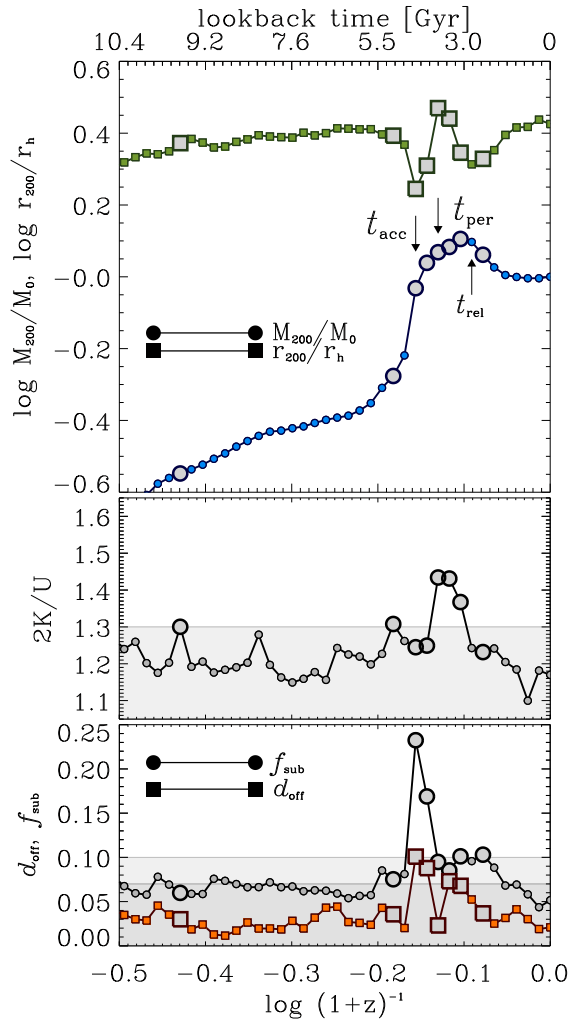


**Figure 2.** An illustrative example of how concentrations vary during the virialization process that follows a major episode of accretion. The upper panel shows, as a function of redshift, the evolution of the virial mass, $M_{200}$, and of the half-mass radius concentration estimator, $r_{200}/r_{\rm h}$, for Aquarius halo F (Springel et al. 2008). This system, which has a half-mass formation redshift of $z_{\rm h} = 0.56$, is in equilibrium at $z = 0$ according to all relaxation criteria, whose evolution is plotted in the bottom two panels. Large symbols are used to indicate times when the halo would not be considered relaxed, according to at least one of the relaxation criteria. Although the halo undergoes a major merger at $z \sim 0.43$, by $z = 0$ more than a crossing time has elapsed, allowing the system to reach equilibrium. During virialization, however, the concentration estimator, $r_{200}/r_{\rm h}$, fluctuates by almost a factor of two. It first reaches a minimum (corresponding to $c \approx 1.6$, assuming an NFW profile) at $t_{\rm acc}$, when the secondary halo first enters the virial radius of the main progenitor, quickly followed by a maximum ($c \approx 12.0$) at $t_{\rm per}$, when the merging subhalo is at first pericentric approach. A second minimum follows next as the accreted material reaches apocenter before relaxing to equilibrium. Recent accretion events can clearly bias concentration estimates unless steps are taken to ensure that halos are relaxed.

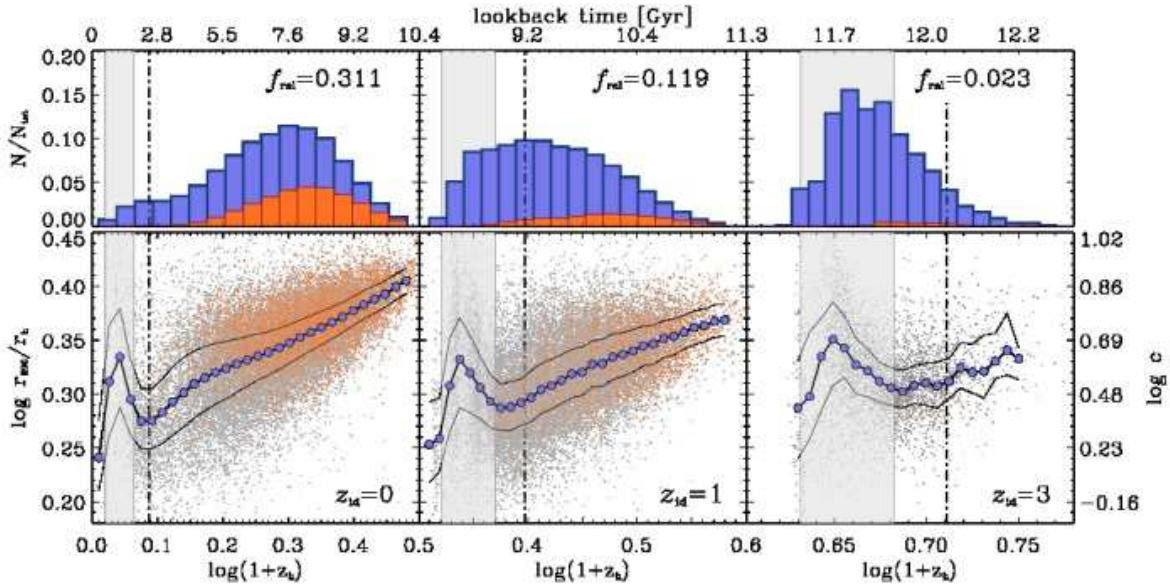


**Figure 3.** *Bottom panels:* Halo concentration, as measured by the virial-to-half mass radius ratio, $r_{200}/r_{\rm h}$, versus half-mass formation redshift, $z_{\rm h}$, for halos in the mass range $3.49 < \log M_{200}/10^{10}h^{-1}M_\odot < 3.79$ and resolved with at least 5000 particles in all Millennium Simulations (see shaded area in Fig. 1). Tickmarks on the right indicate concentration values derived assuming that halos follow NFW profiles. The different panels show halos identified at three different redshifts: $z_{\rm id} = 0$, 1, and 3. Grey dots indicate all halos; orange dots correspond to halos that pass the relaxation criteria specified in Sec. 2.2. The median concentration of the full halo sample is shown by the blue connected circles; thin lines delineate the 25th and 75th percentiles. The shaded area indicate halos whose formation lookback time since identification, $t_{\rm h} = t_{\rm lb}(z_{\rm h}) - t_{\rm lb}(z_{\rm id})$, is between one quarter and three-quarter crossing times, defined as $t_{\rm cross} = 2\,r_{200}/V_{200}$. Halos "formed" more than one crossing time ago (to the right of the dot-dashed vertical line) are in general close to virial equilibrium; for those halos earlier collapse translates into higher concentration. The dependence of concentration on formation redshift becomes non-monotonic when halos that formed less than one crossing time ago are considered, signalling different out-of-equilibrium stages in the virialization process. See text for discussion. *Top panels:* The distribution of formation redshifts for all halos shown in the bottom panels (in blue) and for those satisfying the relaxation criteria (orange). The fraction of relaxed halos in this mass range, $f_{\rm rel}$, decreases with increasing redshift. Very few halos formed less than one crossing time ago pass the relaxation criteria.

If the upturn is driven by unrelaxed halos then we should be able to get some clues to its origin by considering how concentration estimates vary as halos virialize. We turn our attention to this point next.

### 3.2 Concentration estimates and virialization

Massive halos formed hierarchically assemble late and they are therefore expected to have accreted a large fraction of their mass in a short period of time, mainly in the form of major mergers. As a merger proceeds, oscillations in the mass profile drive fluctuations in the concentration as the system relaxes to equilibrium.

We illustrate this in Fig. 2, where we show the evolution of a dark matter halo that undergoes a late-time merger. The system chosen for this illustration is halo Aq-F from the Aquarius Project (Springel et al. 2008). The top panel of Fig. 2 shows the evolution of the virial mass of the most massive progenitor, normalized to the mass at $z = 0$, as well as that of $r_{200}/r_{\rm h}$. The bottom two panels monitor the dynamical relaxation criteria introduced above; when at least one of them fails (i.e., strides outside the shaded areas) the halo would be deemed unrelaxed. We use larger symbols to indicate the times along the evolution when this happens.

Fig. 2 shows that Aq-F undergoes a major merger with a massive secondary halo ("subhalo", for short) at $z \sim 0.4$. Different evolutionary stages are easily identified: the merger begins at $z_{\rm acc} = 0.43$, when the subhalo first enters the virial radius of Aq-F; it reaches pericenter shortly thereafter at $z_{\rm per} = 0.35$. The subhalo is largely disrupted then, and the remnant halo bounces once more before quickly virializing afterward.

The effect of these oscillations on the concentration are shown by the solid squares that track the evolution of $r_{200}/r_{\rm h}$ in the top panel of Fig. 2. Concentrations first drop at $t_{\rm acc}$, reach a maximum at $t_{\rm per}$, and decrease again as the subhalo reaches its second apocenter before settling down. Since first accretion, it takes at least one crossing time (defined as $t_{\rm cross} = 2\,r_{200}/V_{200}$) for the system to virialize. The arrow labelled $t_{\rm rel}$ indicates the moment when one crossing time has elapsed since accretion.

For a system like Aq-F that nearly doubles its virial mass in a merger, the oscillations have large amplitudes: roughly a factor of $\sim 2$ in $r_{200}/r_{\rm h}$, which translates into *a fluctuation of almost one order of magnitude in concentration.* Fig. 2 also shows that the dynamical relaxation criteria introduced above can be effective at identifying systems undergoing these transitions. Unless such criteria are introduced, the average concentration of a halo sample that includes a large fraction of recently-assembled systems may incur substantial bias.

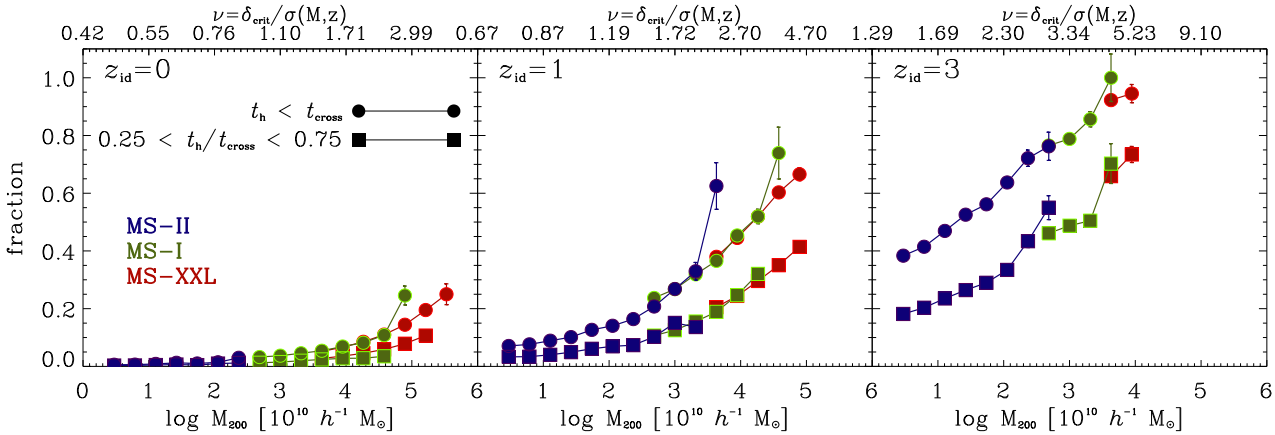


**Figure 4.** Fraction of halos identified at three different redshifts in different stages of relaxation shown as a function of virial mass. The top curves correspond to halos that "formed" less than one crossing time ago; i.e., those where $t_{\rm h} = t_{\rm lb}(z_{\rm h}) - t_{\rm lb}(z_{\rm id}) < t_{\rm cross} = 2\,r_{200}/V_{200}$. These are systems too dynamically young to be in virial equilibrium. The bottom curves in each panel show systems whose formation times suggest that they should have higher-than-average concentrations; i.e., those with $0.25 < t_{\rm h}/t_{\rm cross} < 0.75$ (see shaded area in Fig. 3). Different colours are used to indicate results from MS-I, MS-II, and MS-XXL, as indicated in the legend.

### 3.3 Concentration and formation redshift

Guided by the results discussed in the previous subsection, we explore in Fig. 3 the dependence of concentration on formation redshift. Because halos of different mass collapse on average at different times, we choose halos in the narrow mass range, $3.49 < \log(M_{200}/10^{10}h^{-1}M_\odot) < 3.79$, indicated by the shaded vertical band in Fig. 1. This is close to the characteristic clustering mass at $z = 0$ ($1.35 < \nu < 1.55$), but at $z = 3$ corresponds to the rarest, most massive systems present in the MS-XXL simulation ($4.12 < \nu < 4.73$).

The three panels of Fig. 3 show results for halos identified at $z_{\rm id} = 0$, 1, and 3. The bottom panels show the half-mass radius concentration estimate, $r_{200}/r_{\rm h}$, as a function of the half-mass formation redshift, $z_{\rm h}$, defined as the time when the most massive progenitor first reaches one half of the virial mass of the halo at $z_{\rm id}$. Tickmarks on the right indicate the corresponding NFW-based concentrations. Connected symbols trace the median concentration; thin lines indicate the 25th and 75th percentiles.

The bottom panels of Fig. 3 show that, as expected, halos that form earlier tend to be more concentrated. However, this holds *only* for halos that are "old" enough at the time of identification to have had a chance to relax to equilibrium: the concentration of halos formed less than one crossing-time ago (i.e., $t_{\rm h} = t_{\rm lb}(z_{\rm h}) - t_{\rm lb}(z_{\rm id}) < t_{\rm cross}$) depends non-monotonically on $z_{\rm h}$. (We use $t_{\rm lb}$ to denote cosmic lookback times since $z = 0$.) The median $r_{200}/r_{\rm h}$ trend reverts and has a pronounced maximum when $t_{\rm h} \sim t_{\rm cross}/2$. The same behaviour is observed at all three redshifts, and reflects the oscillations in the structure of halos that have recently accreted a large fraction of their mass as they relax to equilibrium. Halos formed in the period $0.25 < t_{\rm h}/t_{\rm cross} < 0.75$ (highlighted by the shaded area in Fig. 3) are caught at $z_{\rm id}$ during a transient state of maximal concentration.

In general, the more massive the halo the larger the fraction of systems that have assembled recently and that are therefore out of equilibrium. This is shown in the top panels of Fig. 3, where the histograms indicate the distribution of formation redshifts of all clusters (in blue) and of relaxed clusters (in orange). Clearly, very few halos that have assembled less than one crossing time ago pass the relaxation criteria. Indeed, at $z = 3$, when halos in this mass range are very rare the majority are less than one crossing time "old" and fewer than 3% of them are deemed to be in equilibrium. In particular, note that at $z = 3$ a large fraction of systems are at the maximally-compressed stage that corresponds to the first pericentric passage of the accreted material, thus increasing the average concentration.

This suggests that the aforementioned upturn in concentration at high masses is due to the increasing prevalence of systems caught during this particular evolutionary stage. We show this explicitly in Fig. 4, where we plot, as a function of virial mass, the fraction of halos with look-back formation times satisfying $t_{\rm h} < t_{\rm cross}$ (solid lines) and $0.25 < t_{\rm h}/t_{\rm cross} < 0.75$ (dashed lines). The former characterizes halos formed too recently to have reached equilibrium; the latter indicates the fraction likely found in a temporary, highly-concentrated state. Although recently-assembled systems of any mass are susceptible to this effect, the increasing fraction of systems in the latter stage with halo mass (or $\nu$) provides clear support for our interpretation of the upturn as driven by systems passing through a short-lived, highly-concentrated stage of their evolution.

Finally, Fig. 4 makes clear that the fraction of clusters out of equilibrium is not just a function of $\nu$, but also of redshift. For example, at $z_{\rm id} = 0$, about 12% of $\nu \sim 2.5$ systems were formed less than one crossing time ago. At fixed $\nu$, this fraction increases to 42% and 69% at $z_{\rm id} = 1$ and $z_{\rm id} = 3$, respectively. This increase in the fraction of "unrelaxed" systems at given $\nu$ explains why Prada et al. (2011) find that the median concentration, at given $\nu$, increases with redshift (see their Fig.7). The origin of this effect may be traced to the mass-dependent shape of the power spectrum. At fixed $\nu$, the higher the redshift the lower the halo mass and the shallower the slope of the mass fluctuation spectrum, $d\log\sigma/d\log M$. Shallower spectra imply faster struc-

ture growth (Efstathiou et al. 1988), implying that, for a given $\nu$, clusters at high-redshift are being assembled comparably "faster" than their lower-redshift counterparts. This increases the out-of-equilibrium fraction with redshift and pushes the median concentration even higher.

## 4 SUMMARY AND CONCLUSIONS

We have analyzed dark matter halos identified at different redshifts in the Millennium Simulation series (MS-I, MS-II, and MS-XXL) to investigate the origin of the recently-reported upturn in the mass-concentration relation of rare, massive halos. We estimate concentrations from the ratio of virial-to-half mass radius, $r_{200}/r_{\rm h}$, assuming that halos follow an NFW profile. Our analysis confirms that, as a function of the dimensionless mass parameter $\nu(M,z) = \delta_{\rm crit}(z)/\sigma(M,z)$, the median concentration declines gradually until it reaches a minimum at $\nu \sim 3$, then increases toward higher values of $\nu$. This upturn, however, is not present when only dynamically-relaxed halos are retained for analysis, a clear indication that out-of-equilibrium effects drive the non-monotonic behaviour of the mass-concentration relation.

Further inspection demonstrates that the upturn is due to systems caught in a state of "maximal compression" coincident with the first pericentric passage of recently-accreted material. This affects primarily halos that have just accreted a large fraction of their mass, and especially those where the lookback time to formation coincides approximately with the time it takes to bring material from the virial radius of the halo to the center, roughly $r_{200}/V_{200}$. The fraction of systems in this transient stage increases systematically with halo mass, causing the upturn in the $M(c)$ relation that becomes manifest at extremely high masses, where maximally-compressed halos dominate.

The non-monotonic nature of the mass-concentration relation illustrates the fact that, due to their recent assembly, *the vast majority of very massive galaxy clusters are generally expected to be out of dynamical equilibrium.* It further warns about the applicability of simple power-law scalings for various observational mass proxies, such as velocity dispersion, X-ray luminosity/temperature, or SZ decrement, especially when applied to the rarest, most massive clusters. Any sample of such systems is likely to be dominated by systems currently out-of equilibrium, implying that deviations from simple power-laws are to be generally expected. Our findings suggest that the transient dynamical state of galaxy clusters must be carefully and explicitly taken into account before cluster studies may be used as reliable tools of precision cosmology.

This paper has been typeset from a TEX/ LATEX file prepared by the author.

## ACKNOWLEDGEMENTS

We would like to thank Simon White, Volker Springel and Gerard Lemson for useful discussion, and the Virgo Consortium for access to the MS data. ADL acknowledges finacial support from the SFB (956) from the Deutsche Forschungsgemeinschaft. REA is supported by Advanced Grant 246797 GALFORMOD from the European Research Council. MB-K acknowledges support from the Southern California Center for Galaxy Evolution, a multi-campus research program funded by the University of California Office of Research.

**Table 1.** Halo sample considered in our analysis. $\rm N_{halos}$ lists the total number of halos with $N_{200} \geqslant 5000$ in each simulation; $\rm N_{rel}$ the total number of "relaxed" halos (see Section 2.2); and $f_{\rm rel}$ is the relaxed halo fraction.

| Run | $z_{\rm id}$ | $\rm N_{halo}$ | $\rm N_{rel}$ | $f_{\rm rel}$ |
|---|---|---|---|---|
| MSII | 0 | 55,152 | 42,395 | 0.803 |
| | 1 | 64,650 | 35,359 | 0.547 |
| | 3 | 48,321 | 10,412 | 0.215 |
| MSI | 0 | 83,196 | 57,782 | 0.695 |
| | 1 | 64,907 | 22,560 | 0.348 |
| | 3 | 6,560 | 402 | 0.061 |
| XXL | 0 | 2,101,739 | 598,603 | 0.285 |
| | 1 | 910,043 | 102,475 | 0.113 |
| | 3 | 4,799 | 112 | 0.023 |

## REFERENCES

Allen S. W., Evrard A. E., Mantz A. B., 2011, ARA&A, 49, 409
Angulo R. E., Springel V., White S. D. M., Jenkins A., Baugh C. M., Frenk C. S., 2012, ArXiv e-prints: 1203.3216
Boylan-Kolchin M., Springel V., White S. D. M., Jenkins A., Lemson G., 2009, MNRAS, 398, 1150
Bullock J. S., Kolatt T. S., Sigad Y., Somerville R. S., Kravtsov A. V., Klypin A. A., Primack J. R., Dekel A., 2001, MNRAS, 321, 559
Cunha C., Huterer D., Frieman J. A., 2009, Phys Rev D, 80, 063532
Davis M., Efstathiou G., Frenk C. S., White S. D. M., 1985, ApJ, 292, 371
Efstathiou G., Frenk C. S., White S. D. M., Davis M., 1988, MNRAS, 235, 715
Eke V. R., Navarro J. F., Steinmetz M., 2001, ApJ, 554, 114
Evrard A. E., Henry J. P., 1991, ApJ, 383, 95
Henry J. P., Evrard A. E., Hoekstra H., Babul A., Mahdavi A., 2009, ApJ, 691, 1307
Kaiser N., 1986, MNRAS, 222, 323
Kaiser N., 1991, ApJ, 383, 104
Klypin A. A., Trujillo-Gomez S., Primack J., 2011, ApJ, 740, 102
Mantz A., Allen S. W., Ebeling H., Rapetti D., 2008, MNRAS, 387, 1179
Navarro J. F., Frenk C. S., White S. D. M., 1995, MNRAS, 275, 720
Navarro J. F., Frenk C. S., White S. D. M., 1996, ApJ, 462, 563
Navarro J. F., Frenk C. S., White S. D. M., 1997, ApJ, 490, 493

Neto A. F., Gao L., Bett P., Cole S., Navarro J. F., Frenk C. S., White S. D. M., Springel V., Jenkins A., 2007, MNRAS, 381, 1450

Planck Collaboration Aghanim N., Arnaud M., Ashdown M., Aumont J., Baccigalupi C., Balbi A., Banday A. J., Barreiro R. B., Bartelmann M., et al. 2011, A&A, 536, A12

Prada F., Klypin A. A., Cuesta A. J., Betancort-Rijo J. E., Primack J., 2011, ArXiv e-prints: 1104.5130

Rozo E., Rykoff E. S., Evrard A., Becker M., McKay T., Wechsler R. H., Koester B. P., Hao J., Hansen S., Sheldon E., Johnston D., Annis J., Frieman J., 2009, ApJ, 699, 768

Springel V., Wang J., Vogelsberger M., Ludlow A., Jenkins A., Helmi A., Navarro J. F., Frenk C. S., White S. D. M., 2008, MNRAS, 391, 1685

Springel V., White S. D. M., Jenkins A., Frenk C. S., Yoshida N., Gao L., Navarro J., Thacker R., Croton D., Helly J., Peacock J. A., Cole S., Thomas P., Couchman H., Evrard A., Colberg J., Pearce F., 2005, Nature, 435, 629

Springel V., White S. D. M., Tormen G., Kauffmann G., 2001, MNRAS, 328, 726

Vikhlinin A., Kravtsov A. V., Burenin R. A., Ebeling H., Forman W. R., Hornstrup A., Jones C., Murray S. S., Nagai D., Quintana H., Voevodkin A., 2009, ApJ, 692, 1060

Wechsler R. H., Bullock J. S., Primack J. R., Kravtsov A. V., Dekel A., 2002, ApJ, 568, 52

Zhao D. H., Jing Y. P., Mo H. J., Börner G., 2003, ApJL, 597, L9